

Numerical study of Lagrangian velocity structure functions using acceleration statistics and a spatial-temporal perspective

Rohini Uma-Vaideswaran¹ and P. K. Yeung²

¹*School of Aerospace Engineering,
Georgia Institute of Technology, Atlanta, GA 30332, USA**
²*Schools of Aerospace Engineering and Mechanical Engineering,
Georgia Institute of Technology, Atlanta, GA 30332, USA*

(Dated: December 22, 2025)

Abstract

A fundamental relation in Lagrangian Kolmogorov theory is concerned with inertial range scaling of the second-order velocity structure function over intermediate time lags at sufficiently high Reynolds numbers. However, the scaling is not well observed, and it is uncertain whether the scaling constant (C_0) truly approaches a constant value at asymptotic Reynolds numbers. In this paper, direct numerical simulation of forced isotropic turbulence at Taylor-scale Reynolds numbers between 140 and 1300 is used to help advance understanding in this subject. Uncertainties arising from modest simulation time spans are addressed by expressing the velocity structure function in terms of the acceleration autocorrelation, which suggests that C_0 may be sensitive to intermittency effects, leading to a sustained, although weak, Reynolds number dependence. The Lagrangian velocity increment is examined from a spatial-temporal perspective, as a combination of convective (spatial) and local (temporal) contributions, which are subject to a strong but incomplete mutual cancellation dependent on Reynolds number and time lag. The convective increment is strongly influenced by the particle displacement, which is driven by large-scale dynamics and can thus grow into inertial range dimensions in space within just a few Kolmogorov time scales, without fully satisfying classical Lagrangian inertial-range requirements. An overall conclusion in this work is that both the limited range of time scales (narrower than for length scales) and the effects of particle displacements have significant roles in the observed behavior of the second-order Lagrangian velocity structure function.

* rvaideswaran3@gatech.edu

I. INTRODUCTION

It is well known that important and complementary insights about turbulence can be obtained from both the Eulerian viewpoint of a fixed observer and the Lagrangian viewpoint of an observer moving with the instantaneous flow. In particular, two fundamental quantities are the Eulerian and Lagrangian velocity increments, i.e.,

$$\Delta_r \mathbf{u} = \mathbf{u}(\mathbf{x} + \mathbf{r}) - \mathbf{u}(\mathbf{x}), \quad (1)$$

$$\Delta_\tau \mathbf{u}^+ = \mathbf{u}^+(t + \tau) - \mathbf{u}^+(t), \quad (2)$$

where \mathbf{r} is a separation vector, τ is a time lag, the superscript $+$ denotes quantities following particle trajectories, and explicit dependence on time t in Eq. 1 may be omitted if the turbulence is statistically stationary. Statistics of $\Delta_r \mathbf{u}$ are crucial to the classical Kolmogorov similarity hypotheses [1](K41 for short) and refinements therefrom [2–4], while the statistics of $\Delta_\tau \mathbf{u}^+$ are crucial in many attempts to extend K41 theory [5] and/or to develop intermittency corrections [6, 7] for Lagrangian quantities where applicable. The properties of $\Delta_\tau \mathbf{u}^+$ are also crucial for stochastic modeling, where a key task is to predict the statistics of $\mathbf{u}^+(t + \tau)$ when given $\mathbf{u}^+(t)$, with modeling of the particle acceleration $\mathbf{a}^+(t)$ being crucial for capturing Reynolds number dependence [8].

Due to challenges in both experiments and simulations, despite the importance of the subject, the statistics of $\Delta_\tau \mathbf{u}^+$ are less well characterized or understood than those of $\Delta_r \mathbf{u}$. A prime example is the second-order Lagrangian structure function $D_2^L(\tau) = \langle (\Delta_\tau \mathbf{u}^+)^2 \rangle$, where angled brackets denote averaging over a large particle population, and stationarity in time implies $D_2^L(\tau)$ is a function of τ only. For isotropic (including locally isotropic) turbulence, direct use of K41 theory predicts

$$\frac{1}{3} \langle (\Delta_\tau \mathbf{u}^+)^2 \rangle = C_0 \langle \epsilon \rangle \tau, \quad (\tau_\eta \ll \tau \ll T_L), \quad (3)$$

where $\langle \epsilon \rangle$ is the mean energy dissipation rate, τ_η is the Kolmogorov time scale, T_L is the Lagrangian integral time scale of the particle velocity, and C_0 is called the Lagrangian Kolmogorov constant, which is supposedly universal at sufficiently high Reynolds numbers. However, in practice, plots of $\frac{1}{3} \langle (\Delta_\tau \mathbf{u}^+)^2 \rangle / (\langle \epsilon \rangle \tau)$ typically (e.g., in [9, 10]) do not exhibit a distinct plateau. Instead, most data sources show a smooth local peak, with some sensitivity to Reynolds number, in the range of 5–10 τ_η . As the Reynolds number and hence the time-scale ratio T_L/τ_η increases, this range apparently satisfies the criterion $\tau_\eta \ll \tau$ less clearly than it does for $\tau \ll T_L$ [11]. Lagrangian quantities also tend to show stronger intermittency, which is clear from many studies [12–14] showing the fluid particle acceleration (proportional to $\Delta_\tau \mathbf{u}^+$ when τ is small) having a stronger propensity for extreme values than known for Eulerian velocity gradients in space.

In this paper, our goal is to advance understanding of the observed behavior of the Lagrangian second-order structure function in (forced) stationary isotropic turbulence, by employing two complementary approaches. The first approach is to consider the velocity increment as the integral of the fluid particle acceleration, which gives a double integral (for each coordinate component)

$$\langle (\Delta_\tau u^+)^2 \rangle = \int_0^\tau \int_0^\tau \langle a^+(t + t') a^+(t + t'') \rangle dt' dt'', \quad (4)$$

where, by stationarity, the result is independent of the reference time t . This expression is similar in spirit to a formula that gives mean-square displacement in terms of the velocity autocorrelation, dating back to Taylor [15]. The form of the integral implies that both the variance and autocorrelation of the acceleration have important roles in the statistics of the Lagrangian velocity increment, potentially over a substantial period of time.

The second approach is to consider $\Delta_\tau \mathbf{u}^+$ as a spatial-temporal increment, recognizing that $\mathbf{u}^+(t + \tau)$ differs from its prior value $\mathbf{u}^+(t)$ for two reasons, namely that, during the time interval τ , (a) the instantaneous Eulerian velocity field has evolved in time, while (b) the particle has moved to a new location $\mathbf{x}^+(t + \tau)$. In particular, we may write

$$\Delta_\tau \mathbf{u}^+(t) = [\mathbf{u}(\mathbf{x}^+(t + \tau), t + \tau) - \mathbf{u}(\mathbf{x}^+(t), t + \tau)] + [\mathbf{u}(\mathbf{x}^+(t), t + \tau) - \mathbf{u}(\mathbf{x}^+(t), t)] , \quad (5)$$

where the first square bracket on the r.h.s is a spatial increment over a length scale corresponding to the particle displacement $\ell(\tau) = |\mathbf{x}^+(t + \tau) - \mathbf{x}^+(t)|$, and the second is a purely temporal increment taken at the particle's prior position $\mathbf{x}^+(t)$. We refer to these as convective and local increments, respectively. The former is more complex than the Eulerian spatial increment $\Delta_r \mathbf{u}$, because the particle displacement $\ell(\tau)$ is a random variable whose values can spread over a wide range of scales. Since advective transport is driven by the large scales, even in a short time ($\mathcal{O}(\tau_\eta)$), fluid particles can move by a distance much larger than η , causing the convective increment to quickly pick up samples with spatial separations in the inertial range or even beyond. The particle displacement, together with the random-sweeping hypothesis by Tennekes [16], is thus an important parameter in the underlying physics.

In this paper, we present results from direct numerical simulations (DNS) of forced isotropic turbulence. The Taylor-scale Reynolds number range covered is from 140 to 1300, which may be considered to provide [17] reasonable representation of inertial range behavior for Eulerian statistics, although a higher Reynolds number is necessary for the corresponding Lagrangian scaling [10]. It will be seen that, due to computational resources being finite, the time span of some of our higher-resolution simulations are quite modest — but we will show that the key conclusions in this paper are not significantly compromised by this limitation. An analysis of the statistics of the Lagrangian velocity increment in terms of the fluid particle acceleration provides some understanding why the scaling suggested in Eq. (3) is unlikely to hold perfectly even at high Reynolds numbers. The apparently strong yet incomplete cancellation between convective and local contributions to the velocity increment is studied using conditional sampling, which provides a physical mechanism for the emergence of strong intermittency in $\Delta_\tau \mathbf{u}^+$. In addition, the statistics of distance traveled by a fluid particle over a time period τ also helps explain why any plateau resembling Eq. (3) is likely to be quickly truncated.

The remaining sections are organized as follows. In Sec. II, we provide information on the numerical approach and the Lagrangian simulation database. Sec. III contains results on the velocity structure function and an analysis addressing the role of the acceleration autocorrelation. In Sec. IV, we focus on a spatial-temporal perspective and the role of particle displacements on Lagrangian intermittency. Conclusions are summarized in Sec. V.

II. COMPUTATIONAL APPROACH AND SIMULATION OVERVIEW

We have performed DNS using well-known Fourier pseudo-spectral methods for 3D forced isotropic turbulence on an N^3 periodic domain [18]. The forcing scheme used is that of [19] where the energy spectrum (but not individual Fourier modes) at the lowest few wavenumber shells is frozen in time. The fluid particle velocity is obtained by cubic-spline interpolation [20] from the Eulerian velocity field according to the relation $\mathbf{u}^+(t) = \mathbf{u}(\mathbf{x}^+(t), t)$, while particle positions are advanced in time using a second-order Runge Kutta scheme. Lagrangian time series are written out at intervals of $\tau_\eta/20$ or smaller for subsequent post-processing. A large particle count N_P is important in simulations at higher Reynolds numbers and grid resolutions for better sampling of extreme events (e.g., in the fluid acceleration).

The largest simulations reported here at resolution 12288^3 used 2048 nodes on the supercomputer *Frontera* at the Texas Advanced Computing Center (TACC). To ensure high code performance, particle-related communication costs are minimized by distributing the particles dynamically among multiple parallel processes based on their instantaneous positions [21]. The most expensive interpolation-related operation is the generation of cubic spline coefficients from the Eulerian velocity field, which involves solving tridiagonal systems of simultaneous equations with periodic boundary conditions. In departure from the remote memory-access approach in [21], for greater inter-platform portability, we make spline coefficients near the boundaries of adjacent sub-domains available to each parallel process using ghost layers and one-sided communication. These features have resulted in overall costs depending little on the particle count, with N_p of order 10^8 or 10^9 achieved economically.

The spatial-temporal decomposition in Eq. (5) requires knowledge of quantities of the type $\mathbf{u}(\mathbf{x}^+(t_0), t_0 + \tau)$, which is the particle velocity at the end of a time interval $[t_0, t_0 + \tau]$ but calculated at the particle position at time t_0 . This type of information can be difficult to obtain unless particle positions at prior time instants are retained, which would lead to a heavy burden on computer memory requirements. However, stationarity implies the statistics of $\mathbf{u}(\mathbf{x}^+(t_0), t_0 + \tau)$ depend only on τ , and not t_0 . This allows us to simply set $t_0 = 0$ and store the initial particle positions, while continuing to perform interpolation at those initial positions at later times as the simulation proceeds. Since this approach does not require any additional spline coefficients to be computed, any extra cost is minimal.

N^3	N_P	R_λ	$\langle \epsilon \rangle$	T/τ_η	T/T_L	T_L/τ_η	$k_{max}\eta$
256^3	2 M	140	1.43	162.63	12.0	13.50	1.34
1536^3	54 M	390	1.23	181.93	5.70	31.93	2.07
3072^3	54 M	650	1.44	18.16	0.33	54.49	1.99
6144^3	192 M	1000	1.46	18.27	0.21	87.01	1.99
12288^3	192 M	1300	1.37	9.97	0.09	111.02	2.69

TABLE I. DNS parameters: grid resolution, particle count (in multiples of 1 M = 1024^2), Taylor-scale Reynolds number, mean dissipation rate, simulation time span T in units of τ_η and T_L , the time scale ratio T_L/τ_η , and the non-dimensional resolution parameter $k_{max}\eta$.

Table I provides a brief summary of the parameters of the present simulations. As in [11], the Reynolds number is increased by reducing the viscosity with forcing parameters (that

control the large scales) unchanged. This leads to the mean energy dissipation rate ($\langle \epsilon \rangle$) being largely insensitive to Reynolds number, although, the variations that do occur may be significant enough to introduce ambiguities when $\langle \epsilon \rangle$ is used as a normalizing factor (as in Eq. (3)). We have used mostly values of N that include a single factor of 3, which is conducive for optimal code performance given the hardware characteristics of *Frontera*. Except for the lowest Reynolds number, we have maintained small-scale resolution at the level of $k_{max}\eta$ (where $k_{max} = \sqrt{2}N/3$ is the highest resolvable wavenumber on an N^3 grid after dealiasing) at least 2 (which gives a grid spacing Δx very close to 1.5η).

The main limitation in our higher Reynolds number simulations is their relatively short duration. Ideally, T should be large compared to T_L . Unfortunately, although computer memory and speed have been advancing very fast, the cost of long simulations at the grid resolutions needed at high Reynolds numbers is increasing even faster. Studies of small-scale physics in the Eulerian frame can conceivably be conducted using multiple short simulations with independent initial conditions [22, 23]. However, for Lagrangian calculations there are other considerations. First, since T_L is determined by the forcing parameters, which are held fixed, we can use the same value of T_L for all simulations, including shorter ones where the integral defining T_L is not well-converged. Second, with inertial range scaling being our initial motivation, T should at least extend beyond the range where the normalized structure function displays its peak value (between 5–10 τ_η , per [10]), with the effects of finite T to be examined carefully. As seen in Table 1, our simulations meet this requirement.

III. VELOCITY STRUCTURE FUNCTION AND THE ROLE OF ACCELERATION AUTOCORRELATION

As stated earlier, our main goal is to explain the observed numerical behavior of the second-order Lagrangian velocity structure function, including the value of C_0 in Eq. (3). The universality of C_0 is, in fact, not well established. However, any departure from classical theory is likely weaker than that for the Kolmogorov-scaled acceleration variance, i.e.,

$$a_0 = \frac{1}{3} \langle \mathbf{a} \cdot \mathbf{a} \rangle / (\langle \epsilon \rangle^{3/2} \nu^{-1/2}), \quad (6)$$

(where \mathbf{a} is the acceleration vector and ν is the kinematic viscosity) which is well-known to increase systematically with the Reynolds number [12, 24] as a result of intermittency.

In practice, a reasonable way to estimate C_0 is to plot the second-order Lagrangian function, normalized by $\langle \epsilon \rangle \tau$, and look for the peak value, here denoted by C_0^* , at intermediate time lags. Figure 1(a) shows such a plot, which reaches a smooth peak at a τ/τ_η in the range roughly 5–8. The peak appears to be shifted slightly towards higher τ/τ_η at higher R_λ , but there is no clearly recognizable plateau. In frame (b), we show both the height of this peak, as well as a_0 , versus the Reynolds number. The data on a_0 appear to follow closely a power law of slope 0.25, which is consistent with recent work in the literature [25].

For C_0^* , the data appears to suggest a shallow power law of slope 0.2. This power law is admittedly a weak one: it suggests C_0^* may increase from 7.5 to about 10 if R_λ were to increase by a further factor of eight, from about 1300 to 10,000. However, we should caution that this inference is largely empirical in nature, and the present data points do not rule out the possibility of C_0^* leveling out potentially at a value close to 8 at higher Reynolds numbers, which may be accessible within the next decade of leadership computing.

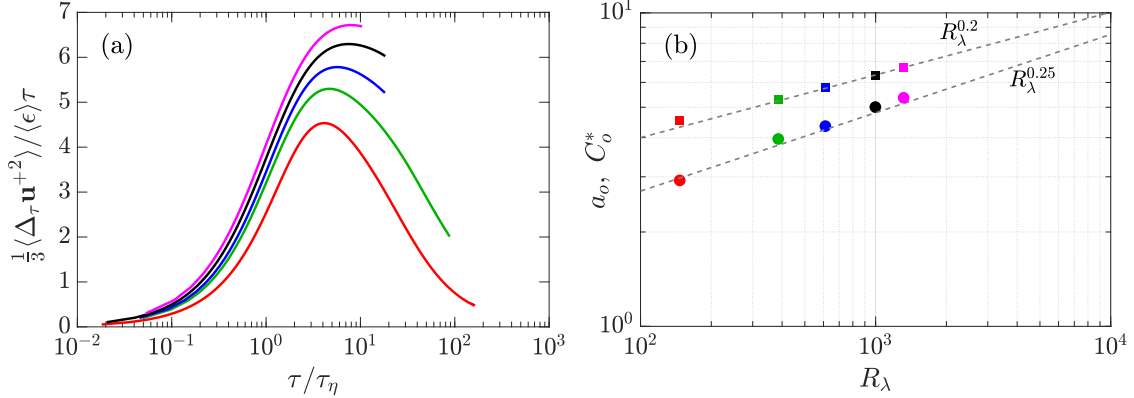


FIG. 1. (a) Normalized second-order Lagrangian structure function at R_λ from 140 to 1300 per Table I (red, green, blue, black, magenta respectively) (b) peak of the curve in (a), denoted by C_0^* (squares) and a_0 (circles). Dashed gray lines indicate power laws fits for comparison: $R_\lambda^{0.2}$ (for C_0^*) and $R_\lambda^{0.25}$ (for a_0).

As noted earlier, the limited time span of some of the higher Reynolds number simulations is a source of statistical uncertainty for both the velocity structure function and its associated autocorrelation function $\rho_L(\tau)$. In particular, the calculation of $\rho_L(\tau)$ for time lags τ comparable to T may involve many temporal increments which are overlapping and therefore lacking in statistical independence, while the ambiguity between so-called biased and unbiased estimators in time-series analysis [26] can also be appreciable. However, a useful check can be made using the acceleration autocorrelation, which has shorter time scales and hence can be obtained more reliably without T being comparable to T_L . In particular, in the same manner as the mean-square displacement being expressible in terms of the velocity autocorrelation, the mean-square of the velocity increment can be expressed in terms of the acceleration autocorrelation as

$$\langle (\Delta_\tau u^+)^2 \rangle = 2\langle a^2 \rangle \int_0^\tau (\tau - s) \rho_a(s) ds \quad (7)$$

$$= 2\langle a^2 \rangle \left[\tau \int_0^\tau \rho_a(s) ds - \int_0^\tau s \rho_a(s) ds \right], \quad (8)$$

which follows from assuming stationarity and performing an integration by parts. We refer to the two integrals in Eq. (8) as I_0 and I_1 respectively. Both are controlled by the shape of the function $\rho_a(s)$, which has a remarkably robust zero-crossing at $s \approx 2.2\tau_\eta$ [13, 27], followed by a negative loop which ends in a slow asymptotic approach to zero. In principle, the negative loop should be consistent with the acceleration having a zero integral time scale, which is a consequence of the acceleration being the time derivative of a stationary process (the velocity). However, if T is not sufficiently long, the integral $\int_0^T \rho_a(s) ds$ will be positive. At small τ , both integrals increase from zero until the zero-crossing of $\rho_a(\tau)$. Subsequently they decrease, with I_0 approaching zero while remaining positive, but in contrast I_1 becomes negative at a small τ , say τ_1 , and eventually approaches a negative constant, consistent with the requirement that $\langle (\Delta_\tau u^+)^2 \rangle$ approaches $2\langle u^2 \rangle$ as $\tau \rightarrow \infty$.

From Eq. (8), multiplying by $1/\tau$ and differentiating with respect to τ , results in

$$\frac{d}{d\tau} \left[\frac{\langle (\Delta_\tau u^+)^2 \rangle}{\tau} \right] = 2\langle a^2 \rangle \frac{1}{\tau^2} \int_0^\tau s \rho_a(s) ds, \quad (9)$$

which indicates the peak of the normalized structure function occurs at $\tau = \tau_1$, where I_1 becomes negative. The peak value itself is given by

$$\langle(\Delta_\tau u^+)^2\rangle/\tau = 2\langle a^2\rangle \int_0^{\tau_1} \rho_a(s) ds. \quad (10)$$

It seems reasonable to suppose the integral $\int_0^{\tau_1} \rho_a(s) ds$ to be mainly determined by information within the first few τ_η , and potentially scale with τ_η itself. If we write

$$\int_0^{\tau_1} \rho_a(s) ds = \gamma \tau_\eta, \quad (11)$$

then normalizing both sides of Eq. (10) by the Kolmogorov variables gives

$$\tilde{C}_0^* = 2 a_0 \gamma, \quad (12)$$

where \tilde{C}_0^* represents C_0^* recovered from $\rho_a(\tau)$ and $\langle a^2\rangle$ for comparison with a direct calculation from the normalized second-order structure function. Since we are expressing velocity increments as integrals of the acceleration, it is not surprising that, due to memory effects, a_0 may have a long-lasting effect on velocity increment statistics and hence the value of \tilde{C}_0^* . We have seen earlier in Fig. 1(b) that, within the data range available, C_0^* increases with Reynolds number, but does so at a slower rate than a_0 . This suggests γ decreases with R_λ .

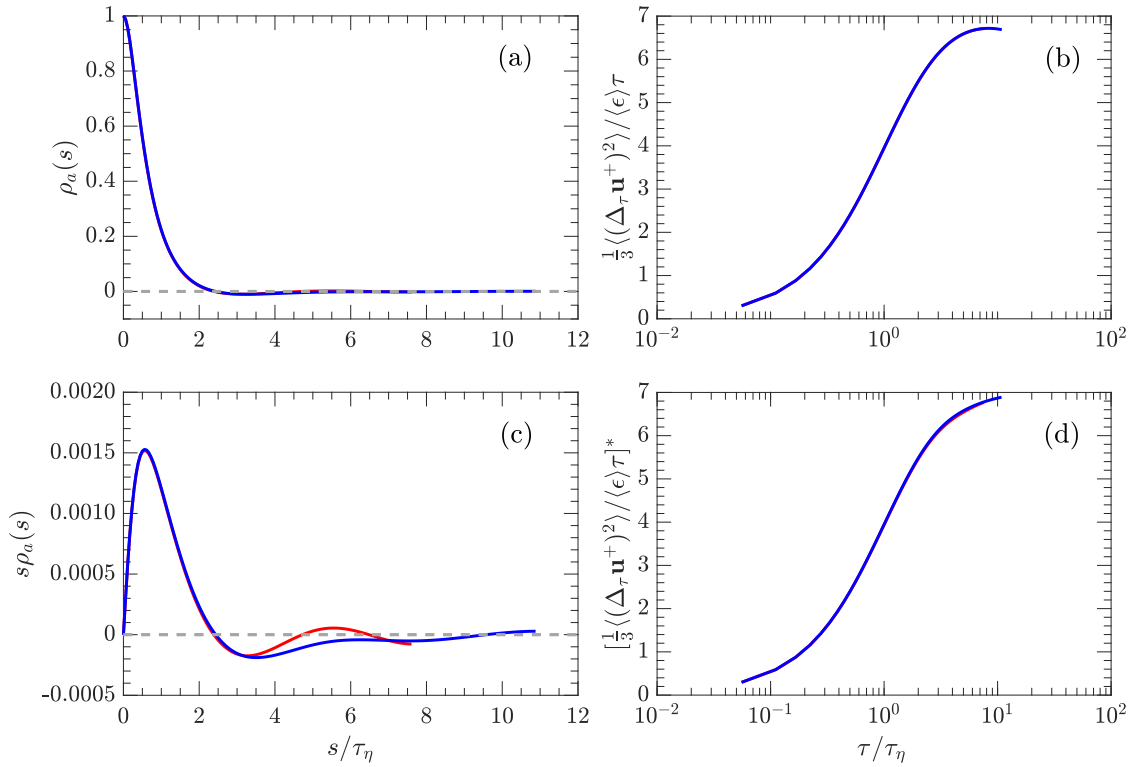


FIG. 2. Results from 12288^3 simulation at the highest R_λ (1300) (a) acceleration autocorrelation and (c) same as (a) but multiplied by time lag; structure function from (b) a direct calculation or (d) recovered from the quantities $\rho_a(\tau)$ and $\langle a^2\rangle$. Lines in red and blue are for data processed up to about $8\tau_\eta$ and $10\tau_\eta$ respectively. (They nearly coincide except in portions of (c).)

It should be noted that accurate calculation of the parameter γ according to Eq. (11) can be challenging if a simulation is limited in length, which can affect the numerical values of $\rho_a(s)$ at larger values of s , and the estimation of τ_1 which sets the upper integration limit. In the two longest (and lowest R_λ) simulations (see Table I) of this work the values of C_0^* and \tilde{C}_0^* differ by less than 1%. However, in the other three shorter but higher R_λ simulations the difference is more noticeable, being 7% in the R_λ 1300 data. In fact, if a simulation is not long enough for the integral I_1 on the r.h.s of Eq. (9) to become negative, accurate estimation of the time lag τ_1 where the peak of the normalized structure function occurs would be difficult.

To assess more closely the impact of the simulation time span on the evaluation of the normalized structure function and its peak, in Fig. 2 we use data at R_λ 1300 to compare statistics obtained by processing only the first 8 τ_η versus the full 10 τ_η . In frame (a), the acceleration autocorrelation appears quite robust — but multiplication by τ (in frame (c)) reveals the presence of significant noise occurring between approximately 4-8 τ_η . This noise, which is more evident if T is short, makes the accurate assessment of γ in Eq. (12) challenging in short simulations. Nevertheless, it is worth noting that the difference apparent between the red and blue lines in frame (b) does not translate into a significant discrepancy between corresponding lines in frame (d). On the other hand, comparison between frames (b) and (d) suggests that in our R_λ 1300 data, \tilde{C}_0^* may be slightly higher than C_0^* , reflecting a limitation associated with short simulation time spans as already discussed.

IV. A SPATIAL-TEMPORAL PERSPECTIVE

Although our main focus is on finite-time increments per Eq. (3), it is clear that at small τ , Eq. (5) gives $\Delta_\tau \mathbf{u}^+ \approx (\mathbf{a}_C + \mathbf{a}_L)\tau$, where $\mathbf{a}_C \equiv (\mathbf{u} \cdot \nabla)\mathbf{u}$ and $\mathbf{a}_L \equiv \partial\mathbf{u}/\partial t$ are, respectively, the convective and local contributions to the material derivative of the velocity in the Navier-Stokes equations. A strong mutual cancellation between \mathbf{a}_C and \mathbf{a}_L is known [27, 28] in accordance with the so-called “random-sweeping” hypothesis by Tennekes [16], which assumes that small-scale turbulence structure is passively advected by the large-scale motions. Recent work [29] focused on the Reynolds number scaling of the statistics of \mathbf{a}_C and \mathbf{a}_L computed as single-time quantities in the Eulerian frame. Also relevant is the work [30] in which, using arguments based on single particle dispersion and random-sweeping, the authors showed that Lagrangian velocity increment statistics arise from the mixing of Eulerian increments over a wide range of scales through an effective Lagrangian dispersion. Here, we focus specifically on the spatial-temporal character of the Lagrangian velocity increment.

A. Random-sweeping and mutual cancellation of the velocity increments

We denote the convective and local velocity increments defined in Eq. (5) by $\mathbf{v}_C(\tau)$ and $\mathbf{v}_L(\tau)$, respectively, such that

$$\Delta_\tau \mathbf{u}^+(\tau) = \mathbf{v}_C(\tau) + \mathbf{v}_L(\tau). \quad (13)$$

At small τ , $\mathbf{v}_C(\tau)$ and $\mathbf{v}_L(\tau)$ are subject to the same strong (but incomplete) mutual cancellation as noted for the convective and local accelerations above. Clearly, the rate of growth of $\Delta_\tau \mathbf{u}^+$ with time lag τ is sensitive to how the degree of mutual cancellation changes, which

in turn is governed by the nature of the joint statistical distribution of the vectors \mathbf{v}_L and \mathbf{v}_C , including their degree of geometric alignment.

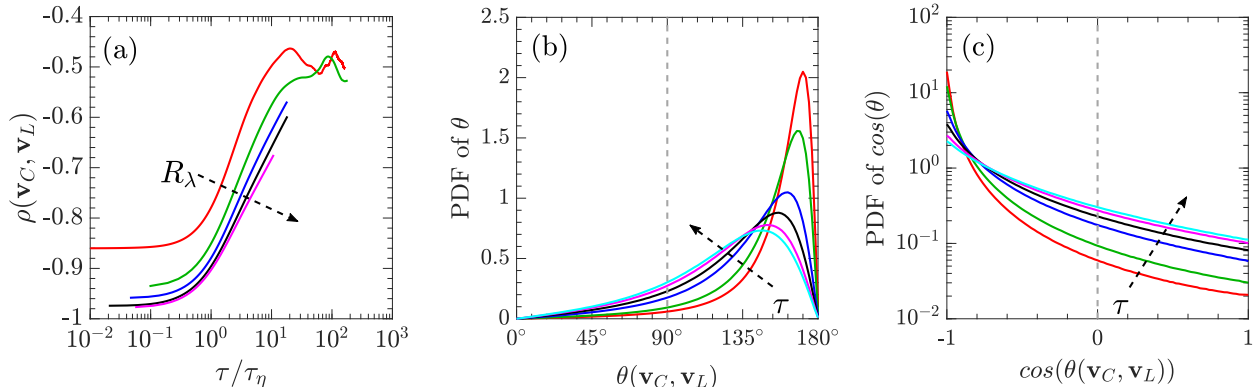


FIG. 3. (a) Evolution of $\rho(\mathbf{v}_L, \mathbf{v}_C)$ in time at R_λ 140, 390, 650, 1000, 1300 (increasing in the direction of the arrow), (b) and (c) PDFs of θ , and $\cos(\theta)$ respectively, at R_λ 390 and time lags $\tau/\tau_\eta \approx 1, 2, 4, 8, 16, 32$, (in the order red, green, blue, black, magenta, cyan).

Figure 3 shows (a) how the correlation coefficient $\rho(\mathbf{v}_C, \mathbf{v}_L)$ evolves with Kolmogorov-scaled time lag at different Reynolds numbers, and (b, c) how the PDFs of the alignment angle θ between \mathbf{v}_C and \mathbf{v}_L (and its cosine) at a given Reynolds number evolves for τ ranging from smaller than τ_η to comparable to T_L . Initially, $\rho(\mathbf{v}_C, \mathbf{v}_L)$ is close to -1.0 , with the alignment angle having a high probability of being close to 180° , which is especially true at higher R_λ . However, since random-sweeping depends on a disparity of scales, it is expected to become weaker as the time lag increases and the velocity increments begin to reach beyond the dissipative scales. Indeed, the degree of anti-correlation begins to weaken noticeably from $\tau \approx 0.5\tau_\eta$ onwards, eventually reaching an asymptotic level close to -0.5 . This asymptotic level can be explained by noting that, at sufficiently large τ , $\mathbf{u}(\mathbf{x}^+(t+\tau), \tau)$, $\mathbf{u}(\mathbf{x}^+(t), t)$ and $\mathbf{u}(\mathbf{x}^+(t), t+\tau)$ are all mutually uncorrelated with each other — such that the covariance $\langle \mathbf{v}_C \cdot \mathbf{v}_L \rangle$ approaches $-\langle u^2 \rangle$ while the variances of both \mathbf{v}_C and \mathbf{v}_L approach $2\langle u^2 \rangle$. The alignment angle PDFs also show that a small but non-trivial number of samples exist, where θ is acute and the alignment is positive.

Although the degree of mutual cancellation between \mathbf{v}_L and \mathbf{v}_C at small τ is strong, complete cancellation is not possible since \mathbf{v}_C contains irrotational contributions but \mathbf{v}_L does not, and also because complete cancellation would result in a zero total acceleration. In addition, the observations from Fig. 3 are subject to the caveats that (because of non-Gaussianity) correlation coefficients do not provide a full picture of how \mathbf{v}_L and \mathbf{v}_C depend on each other statistically, and that statistics on alignment angles do not distinguish between events where the magnitudes of \mathbf{v}_L and \mathbf{v}_C may be large or small.

For a deeper understanding of the joint statistics of \mathbf{v}_L and \mathbf{v}_C , we can examine the conditional PDFs of each variable given the other, at different values of τ/τ_η . Figure 4 shows representative results at R_λ 390. Although conditional PDFs can be very noisy, here, we need only focus on fluctuations on the order of several r.m.s values. If mutual cancellation is complete, then the PDF of \mathbf{v}_C given \mathbf{v}_L should show a sharp spike at $\mathbf{v}_C = -\mathbf{v}_L$, or $v'_C = -(\sigma_C/\sigma_L)v'_L$ when normalization by the respective unconditional r.m.s values (denoted by σ_C and σ_L) is taken into account. However, such sharp spikes are not well observed. Even at small τ , although large values of the conditioning variables lead to the other variable

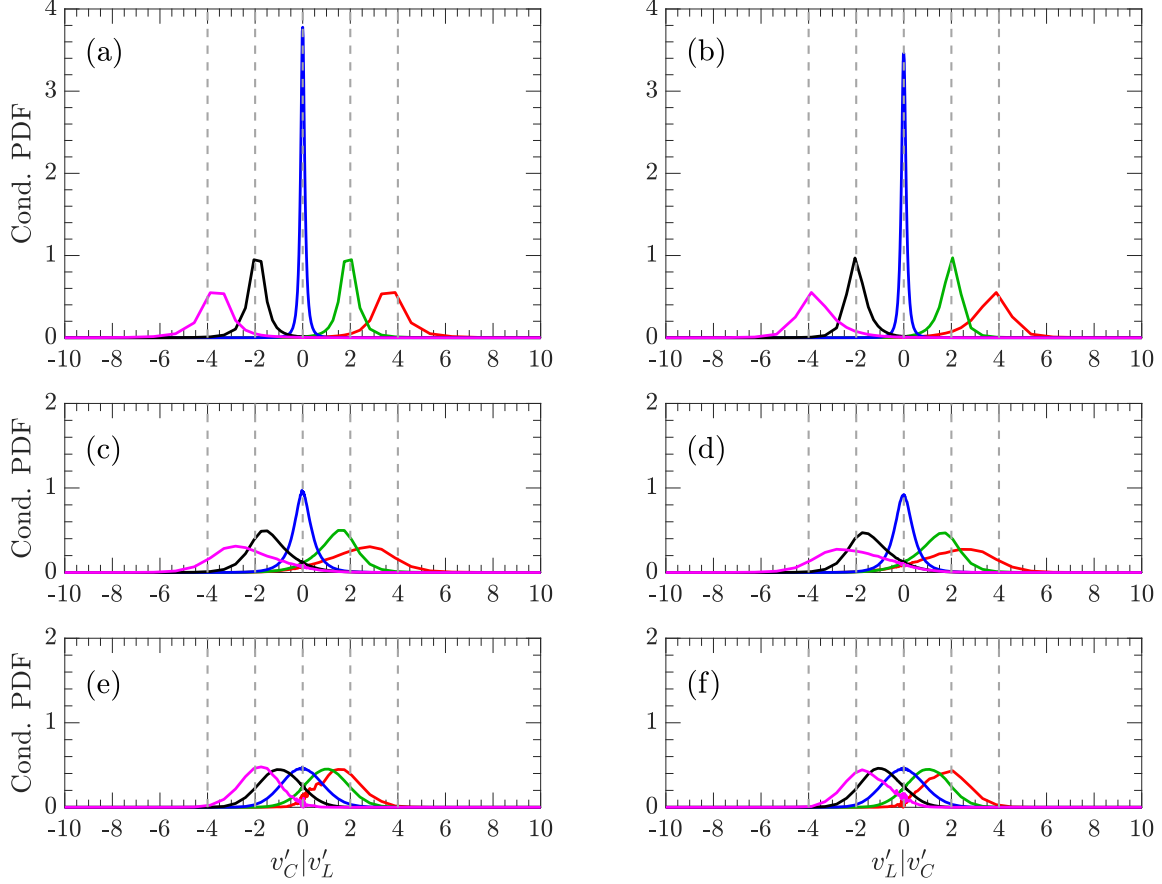


FIG. 4. Conditional PDFs of v'_C given v'_L (left column) and v'_L given v'_C (right column), with primes denoting normalization by unconditional root-mean-square (r.m.s.), using data at R_λ 390 on a 1536^3 grid. Each frame consists of 5 lines, with the conditioning variable at $-4, -2, 0, 2, 4$ times the r.m.s values (red, green, blue, black, magenta) from the mean. Top, middle, and bottom rows show results at $\tau/\tau_\eta \approx 0.1, 4$ and 100 , respectively.

taking mostly values of the opposite sign, the conditional PDFs are spread out over a finite range instead of a narrow spike. The magenta line of frame (b) shows a slight bias towards smaller values of v'_C when conditioned on v'_L , suggesting that \mathbf{v}_L and \mathbf{v}_C do not have the same statistics. As τ increases and the anti-correlation between \mathbf{v}_L and \mathbf{v}_C weakens, the spikes in blue gradually fade. However, close observation of data at larger values of the conditioning variable (lines in red and magenta in frames (e) and (f)) show samples do exist where the two increments are of the same sign. Comparison between lines in red or magenta in frames (a,c,e) or (b,d,f) also show that, as τ increases, any preferential association between large \mathbf{v}_L and large \mathbf{v}_C is gradually lost. The conditional PDFs of \mathbf{v}_C given \mathbf{v}_L and of \mathbf{v}_L and \mathbf{v}_C appear to differ appreciably only at very small τ , where intermittency is the strongest.

Figure 5 shows results similar to the top row of Fig. 4, but at a substantially higher R_λ (1300). The most noticeable contrast is that the spike at early times given near-zero values of the conditioning variable has become taller as well as narrower. This enhanced spike is consistent with prior findings that the random-sweeping hypothesis holds better at higher R_λ . The bias noted above in Fig. 4(b) is also apparently weaker as R_λ increases.

In the discussion of Figs. 4-5 we have focused on samples of \mathbf{v}_C and \mathbf{v}_L in the order of

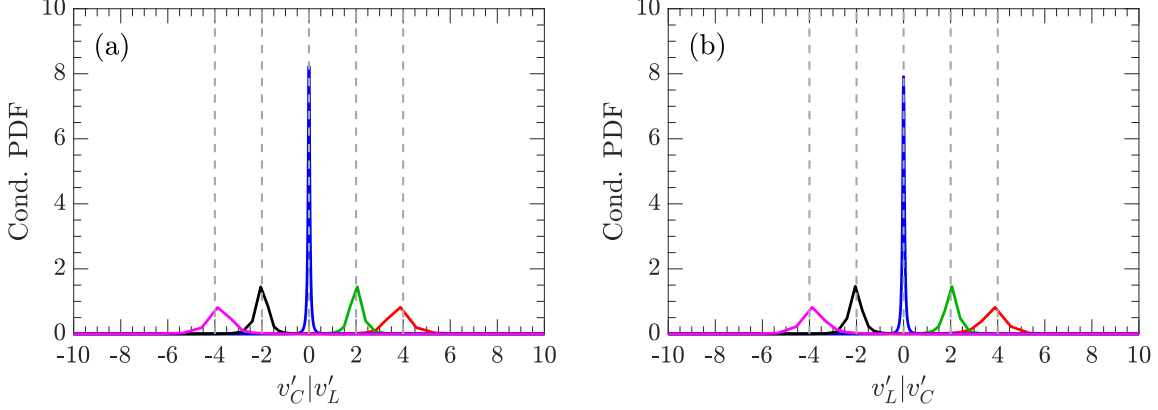


FIG. 5. Same as top row Fig. 4, but for data at R_λ 1300, on a 12288^3 grid.

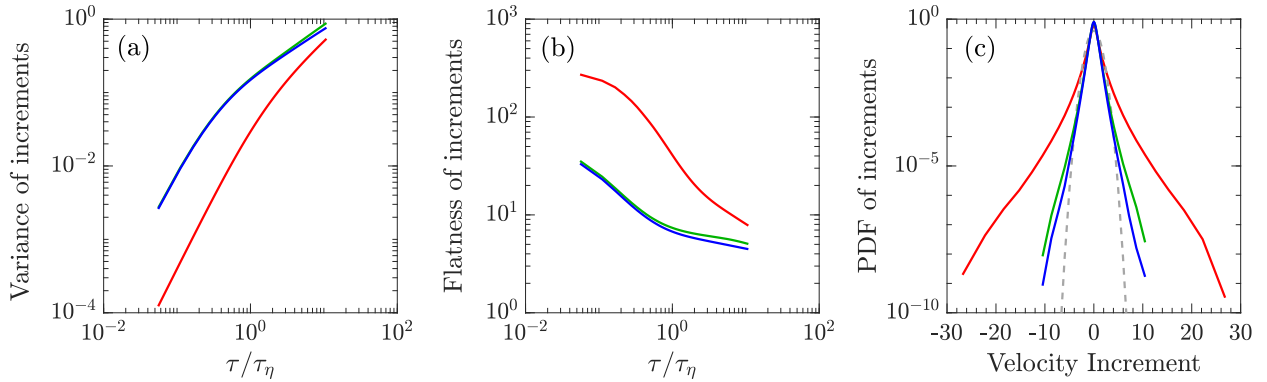


FIG. 6. (a) Variance, (b) Flatness factor and (c) PDF (at $\tau/\tau_\eta \approx 4$) of the Lagrangian velocity increment (red), and its convective (green) and local (blue) contributions at R_λ 1300.

several standard deviations, which provide dominant contributions to lower order moments including variances and covariances. To understand how the mutual cancellation between \mathbf{v}_C and \mathbf{v}_L relate to the evolution of intermittency associated with larger fluctuations, we show in Fig. 6 the dependence on τ for R_λ 1300 data in terms of the variance and flatness factor of $\Delta_\tau \mathbf{u}^+$, \mathbf{v}_C and \mathbf{v}_L , as well as the PDFs of all three increments at a selected time lag. The flatness factor is high at small τ and decreases with τ towards the Gaussian limit (3.0) for all three increments, showing that extreme samples primarily occur at short time lags, in agreement with the small τ limit of $\Delta_\tau \mathbf{u}^+ \approx (\mathbf{a}_C + \mathbf{a}_L)\tau$. We also see that, in accordance with prior findings for the Lagrangian acceleration \mathbf{a} and its contributions \mathbf{a}_C and \mathbf{a}_L [28] the total increment $\Delta_\tau \mathbf{u}^+$ is more intermittent than both \mathbf{v}_C and \mathbf{v}_L , although, the contrast becomes weaker as τ increases. The statistics of \mathbf{v}_C and \mathbf{v}_L are very similar, but \mathbf{v}_C is slightly more intermittent than \mathbf{v}_L . It is thus not surprising that, when forming $\Delta_\tau \mathbf{u}^+$, large values of \mathbf{v}_L are prone to be canceled out by accompanying similarly large or even larger values of \mathbf{v}_C , while the converse is less probable. The overall result is that some large samples of \mathbf{v}_C and \mathbf{v}_L may survive the mutual cancellation, and in conjunction with the possibility of a positive alignment angle (as seen in Fig. 3), contribute to forming extreme values of $\Delta_\tau \mathbf{u}^+$ despite the overall statistical mutual cancellation effect of random-sweeping. The velocity increment PDFs in frame (c) are taken at $\tau/\tau_\eta \approx 4$, which is close to the time lag where approximate Kolmogorov scaling for the velocity structure function starts. At this time lag, the PDFs of \mathbf{v}_C and \mathbf{v}_L are actually not far from Gaussian, but it is clear that

the PDF of $\Delta_\tau \mathbf{u}^+$ shows much wider tails, with samples detected up to about 25 standard deviations.

A primary finding in this subsection is that, despite the apparent success of Tennekes' random-sweeping hypothesis, mutual cancellation between convective and local contributions to the Lagrangian velocity increment is inherently incomplete, with the incompleteness actually contributing to strong intermittency. In the next subsection, we examine the convective increment in more detail, with a focus on the effect of the particle displacement, as a random parameter in how the convective increment is calculated.

B. The role of particle displacements in Lagrangian structure functions

Let $\ell(\tau)$ be the fluid particle displacement vector, and ℓ be its length, measured over a time increment τ . In isotropic turbulence $\langle \ell^2(\tau) \rangle = \langle \ell_i \ell_i \rangle = 3\sigma_1^2(\tau)$, where each Cartesian component of ℓ has the same variance $\sigma_1^2(\tau)$ and being the integral of a Gaussian-distributed velocity component is thus itself close to Gaussian. As a result, ℓ^2/σ_1^2 has a chi-squared distribution of order 3, while its square root ℓ/σ_1 follows a so-called chi distribution, with its PDF being

$$f_{\ell/\sigma_1}(x) = \frac{1}{\sqrt{2}\Gamma(3/2)} x^2 \exp(-x^2/2), \quad (14)$$

where $\Gamma(\cdot)$ is the Gamma function, and $\Gamma(3/2) = \sqrt{\pi}/2$. We are interested in the probability that ℓ/σ_1 exceeds a certain threshold (say x), which is given by a complementary cumulative distribution function (CCDF) of the form

$$P(\ell/\sigma_1 > x) = 1 - F_{\ell/\sigma_1}(x) = \frac{\Gamma^*(3/2, x^2/2)}{\Gamma(3/2)}, \quad (15)$$

where F_{ℓ/σ_1} is the cumulative distribution function (CDF) of ℓ/σ_1 , and $\Gamma^*(3/2, x^2/2) = \int_{x^2/2}^{\infty} t^{1/2} \exp(-t) dt$ is the upper incomplete gamma function (of order 3/2). The CCDF of the Kolmogorov-scaled displacement ℓ/η can also be obtained by using the relation $P(\ell/\eta > x) = P(\ell/\sigma_1 > ax) = 1 - F_{\ell/\sigma_1}(ax)$ where $a = \eta/\sigma_1$.

It is readily understood that at small times (the ballistic range) $\sigma_1^2 \approx u'^2 \tau^2$ where u' is the r.m.s velocity, while at large times (in the diffusion range) $\sigma_1^2 \approx 2u'^2 T_L \tau$. In the ballistic range we can also compare σ_1 to η by writing

$$\frac{\sigma_1}{\eta} \approx \frac{u' \tau}{\eta} = \frac{u'}{u_\eta} \frac{\tau}{\tau_\eta} \approx \left(\frac{1}{15} \right)^{1/4} \sqrt{R_\lambda} \left(\frac{\tau}{\tau_\eta} \right), \quad (16)$$

where the only assumption required is the standard local isotropy relation $\langle \epsilon \rangle = 15\nu(u'/\lambda)^2$. The appearance of the $\sqrt{R_\lambda}$ factor here implies that, especially at high Reynolds number, the distance traveled can quickly become large compared to the Kolmogorov scale — venturing even into the inertial range — at relatively small τ/τ_η .

Figure 7 shows the CCDFs of ℓ/η at two values of time lags for three Reynolds numbers. It can be seen in Fig. 7(a), that within just 1 τ_η over 50% of the particles have moved by roughly 9 η if R_λ is 140, increasing to almost 30 η if R_λ is 1300. In addition, in the R_λ 1300 simulation within 4 τ_η , 80% of the particles have traveled at least 110 η , which is long enough to meet the requirements for inertial range in many aspects of Eulerian statistics. At later

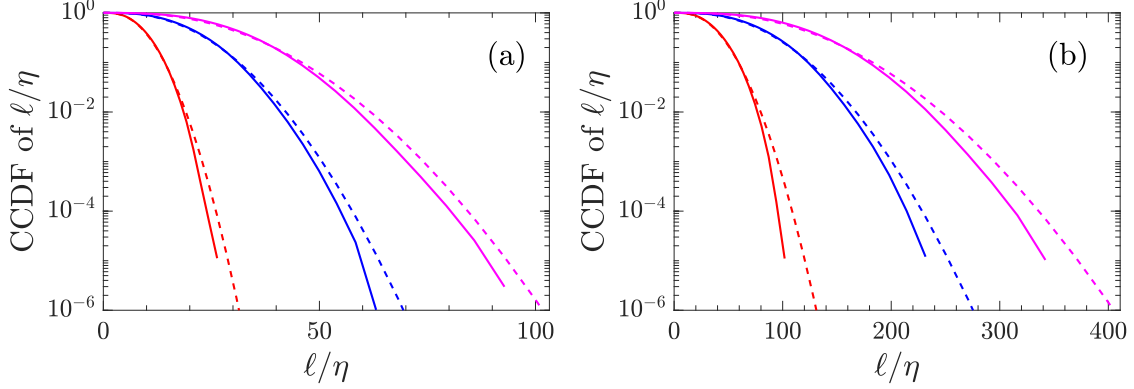


FIG. 7. CCDFs of Kolmogorov-scaled particle displacement ℓ/η from DNS data at R_λ 140 (red), 650 (blue), 1300 (magenta), at $\tau/\tau_\eta \approx 1$ (frame a) and 4 (frame b). Dashed lines represent a theoretical estimate based on Eq. (15).

times, the shift towards larger displacement values slows down somewhat, as a result of σ_1^2 becoming proportional to τ in the diffusive range as opposed to τ^2 in the ballistic range. Nevertheless, at sufficiently large τ many particles will likely have traveled by distances comparable to the integral length scale of the flow. At large ℓ/η , the solid and dashed curves do not fully agree, which can be related to the fact that the independence between different coordinate components assumed in the chi distribution is not guaranteed in actual DNS results where sampling is finite.

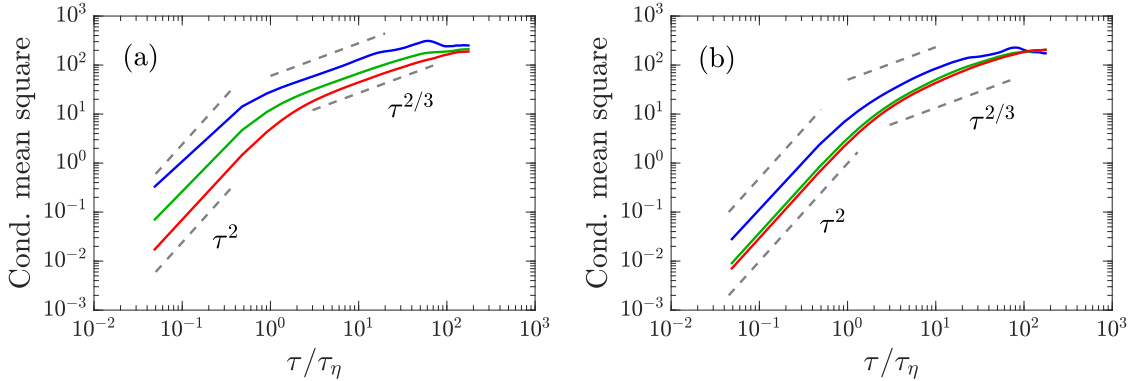


FIG. 8. Conditional mean-square of (a) convective increment and (b) total Lagrangian increment of velocity fluctuations, given displacement $\ell/\langle\ell\rangle$ normalized by instantaneous mean values at close to 1/2 (red), 1 (green), 2 (blue), at R_λ 390. All axes are normalized by Kolmogorov variables. Short dashed lines represent power laws of exponents 2 and 2/3.

To clarify the effect of particle displacements on the statistics of the velocity increments, we have computed the mean squares of \mathbf{v}_C , \mathbf{v}_L and $\Delta_\tau \mathbf{u}^+$ conditioned on the displacement ℓ as a function of τ . Figure 8 shows the conditional mean squares given $\ell/\langle\ell\rangle$ in the neighborhoods of 0.5, 1, and 2, with both axes scaled by Kolmogorov variables, using data from the R_λ 390 simulation, for \mathbf{v}_C and $\Delta_\tau \mathbf{u}^+$ in frames (a) and (b) respectively. In frame (a), the contrasts between lines of different colors indicate that the convective increment increases strongly with $\ell/\langle\ell\rangle$ at most values of τ . For small $\ell/\langle\ell\rangle$, the conditional mean squares of \mathbf{v}_C show regimes of ballistic increase (slope 2 on logarithmic scales) at small τ , inertial range

behavior (slope close to $2/3$ associated with the scaling of Eulerian structure functions) at intermediate τ , and finally slower increases at large τ . However, for larger ℓ , the end of the ballistic regime, the start of the inertial range, and weaker growth at later times, all occur at smaller values of τ/τ_η compared to the case of small ℓ . This contrast is not surprising, since a larger value of ℓ as the conditioning variable implies samples are taken over positions that are further apart. At the same time, with the skewness of the chi distribution for $\ell/\langle\ell\rangle$ being small (~ 0.49), the conditional mean square given $\ell/\langle\ell\rangle \approx 1$ agrees with the unconditional result very well (to within less than 1%, hence not shown here).

Frame (b) of Fig. 8 shows the conditional mean square of the total increment $\Delta_\tau \mathbf{u}^+$ follows similar trends, but also displays some differences. Specifically, ballistic behavior in the blue line is better captured, which is consistent with the effect of large particle displacements in the convective increment being partly canceled by the local increment that also contributes to $\Delta_\tau \mathbf{u}^+$. The sensitivity of the statistics of $\Delta_\tau \mathbf{u}^+$ to $\ell/\langle\ell\rangle$, inferred from the spacings among curves of different colors, is significantly weaker than that seen in the statistics of \mathbf{v}_C (in frame (a)). It is also clear that, regardless of the conditioning $\ell/\langle\ell\rangle$, as τ/τ_η approaches inertial-range values, the scaling of the total increment is more ambiguous, since the spatial-temporal Lagrangian velocity increment scales differently from either the spatial or temporal increments.

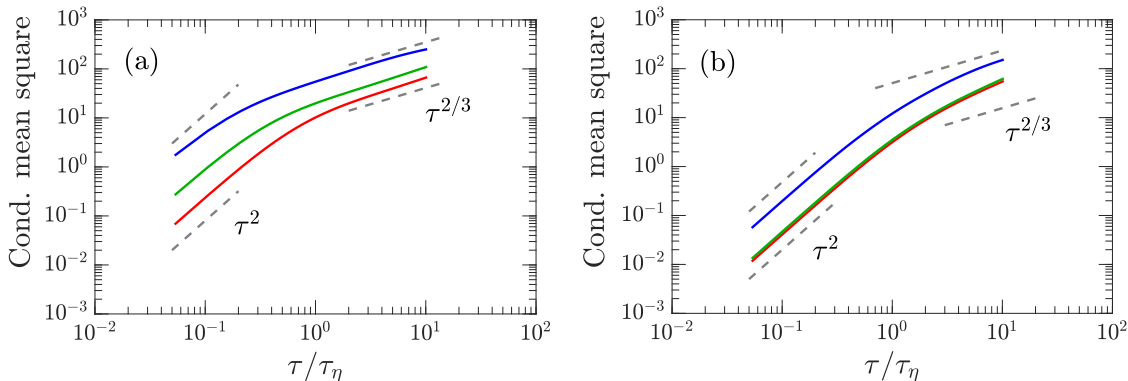


FIG. 9. Same as Fig. 8, but showing data at R_λ 1300.

To assess Reynolds number effects on the conditional statistics, in Fig. 9 we show results at R_λ 1300, where stronger intermittency is accompanied by a time scale ratio T_L/τ_η more than three times larger (per Table I) than that at R_λ 390. In frame (a), even at small τ , the wider range of scales can cause the mean square of \mathbf{v}_C given $\ell/\langle\ell\rangle \approx 2$ (or higher) to depart quickly from ballistic behavior, since such values of ℓ can quickly become much larger than η . However, at intermediate time lags, $\tau^{2/3}$ scaling for R_λ 1300 is noticeably clearer than at R_λ 390. In contrast, the conditional mean square in frame (b) closely resembles that for R_λ 390 in frame (b) of Fig. 8 earlier, except that the R_λ 1300 simulation only reached $10 \tau_\eta$ in time. The relative lack of a convincing power law in the conditional mean squares of $\Delta_\tau \mathbf{u}$ (versus that for \mathbf{v}_C) is also consistent with uncertainties in the application of traditional K41 similarity to the second-order Lagrangian structure function addressed in Sec. III.

The results in Figs. 8 and 9, as discussed above, raise the question of whether the unconditional mean square may also display any scaling ranges of the type observed for the conditional quantities. Since the $\tau^{2/3}$ scalings in the conditional statistics above have been obtained only from fluid particles that have traveled by a certain distance in the inertial

range over a given time interval, their relevance to the global statistics over all the particles depends on the probability of ℓ being in the inertial range (and the extent of such). This probability can be estimated by subtracting between values of the CCDF of ℓ/η corresponding to values of r/η that mark the start and end of the inertial range. For R_λ 1300, based on data on the third-order Eulerian structure functions [17] we can take the inertial range available as $50 \leq r/\eta \leq 400$. The data in Fig. 7 gives the proportion of fluid particles in this range as 5 % at $\tau/\tau_\eta \approx 1$ and 94 % at $\tau/\tau_\eta \approx 4$. The high proportion in the latter case strongly suggests that the unconditional mean square of \mathbf{v}_C should behave similarly as their conditional counterparts in Fig. 9(a).

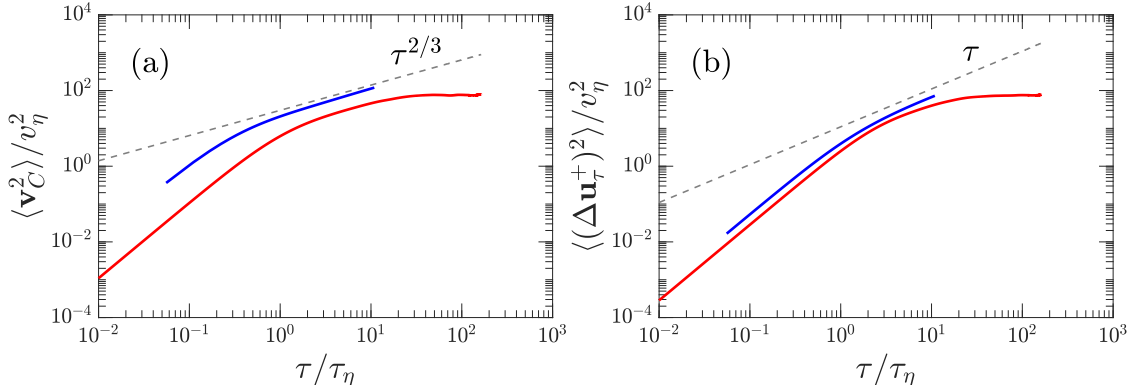


FIG. 10. Evolution of $\langle (\Delta_\tau \mathbf{u}^+)^2 \rangle$ and $\langle \mathbf{v}_C^2 \rangle$ in time at R_λ 140 (red) and 1300 (blue), scaled by Kolmogorov variables. Dotted lines of slope 1 and $2/3$ are shown for comparison.

The connection between the $r^{2/3}$ scaling for the mean-squared spatial velocity increment $\Delta_\tau \mathbf{u}$ in the Eulerian inertial range, and the inertial range scaling for the mean-squared spatial increment \mathbf{v}_C merits some additional discussion. While for sufficiently small τ , a Taylor-series expansion indicates that $\ell \propto \tau$ (statistically), with the proportionality factor being the r.m.s velocity, if τ is several τ_η long, the Taylor series argument may require justification. However, at high R_λ , a time lag of a few τ_η can perhaps still be considered to be small compared to T_L . Thus, if the velocity autocorrelation remains high at the time lags involved, the Taylor series approximation may sufficiently hold. It may also be argued that since power laws are defined by local slopes, the Taylor series argument remains applicable if the question is only whether a portion of the curve showing $\langle \mathbf{v}_C^2 \rangle$, where the ℓ involved corresponds to separations in the Eulerian inertial range, displays the logarithmic slope of $2/3$. In other words, since the convective velocity increment \mathbf{v}_C can be interpreted as a velocity increment over the spatial separation $\ell(\tau)$, its variance should scale as $\tau^{2/3}$ provided ℓ lies in the Eulerian inertial range. The Reynolds number trends observed in Fig. 7 also suggest that such a $\tau^{2/3}$ scaling region would emerge earlier and last longer as R_λ increases.

In Fig. 10 we show the evolution of the unconditional mean-squared (a) convective and (b) total velocity increments scaled by the Kolmogorov variables. For R_λ 1300 the convective increments indeed show $\tau^{2/3}$ behavior — starting from τ/τ_η just slightly beyond 1.0 — for the reasons given above, based on both the Taylor series approximation as well as the conditional mean squares. For R_λ 140 this trend starts later because of u'/u_η being smaller at lower R_λ , so that it takes a larger number of time lags (in units of τ_η) for most particles to have traveled by a distance in the inertial range. This is also consistent with our observation in Fig. 7 that particle displacements reach separations in the inertial range at progressively

smaller τ as the R_λ increases. The R_λ 140 simulation was also sufficiently long (at least in units of τ_η) for the curve to eventually level out when most of the particles are so far apart that $\mathbf{u}(\mathbf{x}^+(t + \tau), t + \tau)$ and $\mathbf{u}(\mathbf{x}^+(t), t + \tau)$ become fully independent. While the R_λ 1300 simulation only reached about $10 \tau_\eta$, the same behavior can be expected at late times, implying that the $\tau^{2/3}$ scaling only lasts for a modest length of time. On the other hand, in frame (b), the scaling that is observed, although only approximately, in the range for several τ_η is τ^1 , which corresponds to the classical K41 result for the second-order Lagrangian structure function. As noted earlier, the dissimilarity between the scaling of the convective and total increments is an indication of the strength of the (partial) mutual cancellation that exists between convective and local contributions. The choice of logarithmic versus linear scales is the main reason why sensitivity to Reynolds number in Fig. 10 looks much weaker than that seen in Fig. 1. We also note in passing that in the ballistic range, all the curves in Fig. 10 scale as τ^2 . The heights at a given small τ/τ_η are proportional to the respective acceleration variances, which increase with Reynolds number. The Reynolds number dependence of $\langle \mathbf{v}_C^2 \rangle$ is also stronger than that of $\langle (\Delta_\tau(\mathbf{u}^+))^2 \rangle$, as reported previously in [28].

The analyses provided in this section show that particle displacement plays a significant role in the scaling of the Lagrangian structure function, which is made clear when viewed in a spatial-temporal framework. However, the strong partial cancellation between the convective and local increments leads to the total Lagrangian velocity increment behaving differently, including showing a different approximate power law at intermediate times.

V. CONCLUSIONS

A well-known prediction from the application of classical Kolmogorov theory in the Lagrangian frame is that the second-order velocity structure function should scale linearly (Eq. (3)) over intermediate time lags (τ), at sufficiently high Reynolds number. However, this scaling is not well observed, and there is significant uncertainty in whether the scaling constant (called C_0) truly approaches universal behavior at asymptotically high Reynolds numbers. Particularly, in direct numerical simulations (DNS), the normalized structure function often possesses a local peak (rather than a plateau) which forms after just 5-10 Kolmogorov time scales (τ_η) but is subsequently quickly truncated. Although, one contributing factor here is that the range of time scales widens more slowly than the range of length scales with increasing Reynolds numbers. In this paper, we have used DNS data in forced isotropic turbulence at Taylor-scale Reynolds numbers (R_λ) 140 to 1300 to help improve understanding in this subject, with connections to the statistics of fluid particle acceleration and the effects of particle displacement ($\ell(\tau)$) from a spatial-temporal perspective.

To assess statistical aspects of uncertainties related to finite simulation time span, we have considered the mean-squared velocity increment as a double integral of the acceleration autocorrelation, whose properties, including a quick zero-crossing followed by a slow return to zero, are well known. This analysis shows that the peak value (C_0^* , in Eq. (12)) of the Kolmogorov-scaled second-order structure function has a strong connection to the Kolmogorov-scaled acceleration variance (a_0), which increases with Reynolds number due to intermittency. It also appears that, in practice, for the type of forced turbulence considered,

a simulation spanning $10 \tau_\eta$ can provide reasonable accuracy for key results including C_0^* in this work. With this caveat, it can be seen that our present results suggest some support for an empirical scaling law of $C_0^* \propto R_\lambda^{0.2}$, only slightly weaker than $R_\lambda^{0.25}$ for the Kolmogorov-scaled acceleration variance, although this result does not rule out the possibility that C_0^* may reach a universal asymptotic value C_0 at much higher Reynolds numbers than currently accessible.

As written in Eq. (5), the Lagrangian velocity increment $\Delta_\tau \mathbf{u}^+$ is inherently a spatial-temporal quantity with convective (\mathbf{v}_C) and local (\mathbf{v}_L) contributions, that are subject to strong yet incomplete mutual cancellation, in agreement with the so-called random-sweeping hypothesis. The partial cancellation results in $\Delta_\tau \mathbf{u}^+$ having a smaller variance but higher intermittency than both \mathbf{v}_C and \mathbf{v}_L , especially at higher Reynolds numbers, although the effect weakens at later times. A more intriguing aspect is the role of the particle displacement, which is well described by a chi distribution of order three. Since $\ell(\tau)$ (i.e., the change of ℓ over any short time interval) scales with the r.m.s velocity u' , changes of ℓ much larger than η can occur even for τ only at a few τ_η . Statistics of convective increments conditioned upon ℓ/η help explain the emergence of a convincing $\tau^{2/3}$ scaling in $\langle \mathbf{v}_C^2 \rangle$, in connection with the $r^{2/3}$ scaling for Eulerian velocity structure functions in the inertial range. For instance, in our data at R_λ 1300, the proportion of samples of ℓ within an estimated inertial range of spatial separations between 50 and 400 Kolmogorov length scales rises from 5% at $\tau/\tau_\eta \approx 1$ to as high as 94% at $\tau/\tau_\eta \approx 4$. This high percentage implies that the mean-square of \mathbf{v}_C behaves similarly to its own conditional value given ℓ in the appropriate scaling range. Finally, although the incomplete cancellation implies that $\langle (\Delta_\tau \mathbf{u})^2 \rangle$ does not follow the same power law, the occurrence of large displacements within short time intervals still helps explain why the structure function starts to exhibit inertial-like scaling as early as a few τ_η , and that the approximate scaling is also quickly washed out as particle displacements begin to exceed inertial scales in space.

In summary, we believe this work provides new insights into the observed behavior and often limited or elusive inertial range scaling for the second-order Lagrangian structure function, including whether the Lagrangian Kolmogorov constant will approach an asymptotic constant value in the limit of very large Reynolds number. A spatial-temporal perspective shows that both the limited range of time scales (compared to length scales) and the time-dependent particle displacements play significant roles. A related open question is how at least some details of the Lagrangian dynamics would differ when particle inertia is taken into account. This question may also be of interest when interpreting experimental data based on following the trajectories of tracer particles, which may not exactly move with the flow.

-
- [1] A. N. Kolmogorov, The local structure of turbulence in an incompressible fluid with very large Reynolds numbers, *Dokl. Akad. Nauk SSSR* **30**, 301 (1941).
 - [2] A. N. Kolmogorov, A refinement of previous hypotheses concerning the local structure of turbulence in a viscous incompressible fluid at high Reynolds number, *J. Fluid Mech.* **13**, 82 (1962).
 - [3] U. Frisch, Turbulence: the legacy of A. N. Kolmogorov (Cambridge University Press, 1995).
 - [4] K. R. Sreenivasan and R. A. Antonia, The phenomenology of small-scale turbulence, *Annu.*

- Rev. Fluid Mech. **29**, 435 (1997).
- [5] A. S. Monin and A. M. Yaglom, Statistical Fluid Mechanics, Vol. 2 (MIT Press, 1975).
 - [6] L. Biferale, E. Bodenschatz, M. Cencini, A. S. Lanotte, N. T. Ouellette, F. Toschi, and H. Xu, Lagrangian structure functions in turbulence: A quantitative comparison between experiment and direct numerical simulation, *Phys. Fluids* **20**, 065103 (2008).
 - [7] H. Yu and C. Meneveau, Lagrangian refined Kolmogorov similarity hypothesis for gradient time evolution and correlation in turbulent flows, *Phys. Rev. Lett.* **104**, 084502 (2010).
 - [8] B. L. Sawford, Reynolds number effects in lagrangian stochastic models of dispersion, *Phys. Fluids A* **3**, 1577 (1991).
 - [9] P. K. Yeung, Lagrangian investigations of turbulence, *Annu. Rev. Fluid Mech.* **34**, 115 (2002).
 - [10] B. L. Sawford and P. K. Yeung, Kolmogorov similarity scaling for one-particle Lagrangian statistics, *Phys. Fluids* **23**, 091704 (2011).
 - [11] P. K. Yeung, S. B. Pope, and B. L. Sawford, Reynolds number dependence of lagrangian statistics in large numerical simulations of isotropic turbulence, *J. Turb.* **7(58)**, 1 (2006b).
 - [12] G. A. Voth, K. Satynarayan, and E. Bodenschatz, Lagrangian acceleration measurements at large Reynolds numbers, *Phys. Fluids* **10**, 2268 (1998).
 - [13] P. K. Yeung, S. B. Pope, E. A. Kurth, and A. G. Lamorgese, Lagrangian conditional statistics, acceleration and local relative motion in numerically simulated isotropic turbulence, *J. Fluid Mech.* **582**, 399 (2007).
 - [14] L. Bentkamp, C. C. Lalescu, and M. Wilczek, Persistent accelerations disentangle lagrangian turbulence, *Nature Communications* **10**, 3550 (2019).
 - [15] G. I. Taylor, Diffusion by continuous moments, *Proc. Lond. Math. Soc.* **20**, 196 (1921).
 - [16] H. Tennekes, Eulerian and Lagrangian time microscales in isotropic turbulence, *J. Fluid Mech.* **67**, 561 (1975).
 - [17] K. P. Iyer, K. R. Sreenivasan, and P. K. Yeung, Reynolds number scaling of velocity increments in isotropic turbulence, *Phys. Rev. E* **95**, 021101 (2017).
 - [18] R. S. Rogallo, Numerical experiments in homogeneous turbulence, NASA Tech. Memo. 81315, NASA Ames Research Center (1981).
 - [19] D. A. Donzis and P. K. Yeung, Resolution effects and scaling in numerical simulations of passive scalar mixing in turbulence, *Physica D* **239**, 1278 (2010).
 - [20] P. K. Yeung and S. B. Pope, An algorithm for tracking fluid particles in numerical simulations of homogeneous turbulence., *J. Comput. Phys.* **79**, 373 (1988).
 - [21] D. Buaria and P. K. Yeung, A highly scalable particle tracking algorithm using partitioned global address space (PGAS) programming for extreme-scale turbulence simulations, *Comput. Phys. Commun.* **221**, 246 (2017).
 - [22] P. K. Yeung and K. Ravikumar, Advancing understanding of turbulence through extreme-scale computation: Intermittency and simulations at large problem sizes, *Phys. Rev. Fluids* **5**, 110517 (2020).
 - [23] P. K. Yeung, K. Ravikumar, R. Uma-Vaideswaran, D. L. Dotson, K. R. Sreenivasan, S. B. Pope, C. Meneveau, and S. Nichols, Small-scale properties from exascale computations of turbulence on a $32,768^3$ periodic cube, *J. Fluid Mech.* **1019**, R2 (2025).
 - [24] P. Vedula and P. K. Yeung, Similarity scaling of acceleration and pressure statistics in numerical simulations of turbulence, *Phys. Fluids* **11**, 1208 (1999).
 - [25] D. Buaria and K. R. Sreenivasan, Lagrangian acceleration and its Eulerian decompositions in fully developed turbulence, *Phys. Rev. Fluids* **8**, L032061 (2023).
 - [26] M. B. Priestley, Spectral Analysis and Time Series (Academic Press, 1983).

- [27] P. K. Yeung and S. B. Pope, Lagrangian statistics from direct numerical simulations of isotropic turbulence, *J. Fluid Mech.* **207**, 531 (1989).
- [28] A. Tsinober, P. Vedula, and P. K. Yeung, Random Taylor hypothesis and the behavior of local and convective accelerations in isotropic turbulence, *Phys. Fluids* **13**, 1974 (2001).
- [29] D. Buaria and K. R. Sreenivasan, Lagrangian acceleration and its Eulerian decompositions in fully developed turbulence, *Phys. Rev. Fluids* **8**, L032601 (2023).
- [30] C. C. Lalescu and M. Wilczek, How tracer particles sample the complexity of turbulence, *New J. Phys.* **20**, 013001 (2018).

ACKNOWLEDGMENTS

The authors acknowledge the Texas Advanced Computing Center (TACC) at The University of Texas at Austin for providing computational resources that have contributed to the research results reported within this paper. URL: <http://www.tacc.utexas.edu>. We also thank Prof. Michael Wilczek for many helpful discussions.